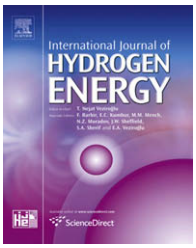
Available at www.sciencedirect.com

ScienceDirect

journal homepage: www.elsevier.com/locate/he



Computational study of metal hydride cooling system

A. Satheesh, P. Muthukumar, Anupam Dewan*

Department of Mechanical Engineering, Indian Institute of Technology, Guwahati, Guwahati 781039, India

ARTICLE INFO

Article history:
Received 13 June 2008
Received in revised form
10 December 2008
Accepted 29 January 2009
Available online 25 February 2009

Keywords:
Metal hydride
Heat pump
Coupled heat and mass transfer

ABSTRACT

A computational study of a metal hydride cooling system working with $MmNi_{4.6}Al_{0.4}$/$MmNi_{4.6}Fe_{0.4}$ hydride pair is presented. The unsteady, two-dimensional mathematical model in an annular cylindrical configuration is solved numerically for predicting the time dependent conjugate heat and mass transfer characteristics between coupled reactors. The system of equations is solved by the fully implicit finite volume method (FVM). The effects of constant and variable wall temperature boundary conditions on the reaction bed temperature distribution, hydrogen concentration, and equilibrium pressures of the reactors are investigated. A dynamic correlation of the pressure–concentration–temperature plot is presented. At the given operating temperatures of 363/298/278 K ($T_H/T_M/T_C$), the cycle time for the constant and variable wall temperature boundary conditions of a single-stage and single-effect metal hydride system are found to be 1470.0 s and 1765.6 s, respectively. The computational results are compared with the experimental data reported in the literature for $LaNi_{4.61}Mn_{0.26}Al_{0.13}$/$La_{0.6}Y_{0.4}Ni_{4.8}Mn_{0.2}$ hydride pair and a good agreement between the two was observed.

© 2009 International Association for Hydrogen Energy. Published by Elsevier Ltd. All rights reserved.

1. Introduction

Metal hydrides can be effectively utilized as working materials in a number of thermal machines which can contribute significantly towards the environmentally clean energy technologies. These systems use low grade thermal energy, for example, waste heat from industries, solar energy and heat from exhaust flue gases to produce high quality thermal energy and cooling outputs. Metal hydride heat pump (MHHP) is one of the promising applications of metal hydrides, which can be tailored to provide heating and cooling or temperature upgrading over a wide range of input and ambient temperatures. Development and optimization of such devices require highly sophisticated computational design methods. The major limitations of these devices are high initial cost of the hydride alloy and difficulty in achieving optimized heat and hydrogen transfer in the reaction bed.

Nishizaki et al. [1] modelled a chemical hydride heat pump consisting of four reactors of $LaNi_{4.7}Al_{0.3}$/$LaNi_5$ hydride pair. They formulated the equation for the coefficient of performance (COP) of MHHP by introducing the sensible heat exchange factor between the reactors. Ron [2] designed and built a MHHP that used waste heat of exhaust gases as the heat source temperature for a bus air-conditioner. Bjurstrom and Suda [3] carried out both experimental and numerical investigations of MHHP. Lee et al. [4] constructed a prototype of a MHHP operating between $Zr_{0.9}Ti_{0.1}Cr_{0.9}Fe_{1.1}$ as high temperature and $Zr_{0.9}Ti_{0.1}Cr_{0.6}Fe_{1.4}$ as low temperature alloys. They found that the plateau pressure and reaction kinetics could be controlled by changing the relative composition of Cr and Fe. Gopal and Murthy [5] numerically investigated a single-stage metal hydride cooling system working with ZrMnFe/$MmNi_{4.5}Al_{0.5}$ hydride alloy pair using a one-dimensional model. They studied the performance characteristics of

* *Corresponding author*. Tel.: +91 361 2582673; fax: +91 361 2690762.
E-mail addresses: pmkumar@iitg.ernet.in, pmuthukkumar@yahoo.com (P. Muthukumar).
0360-3199/$ – see front matter © 2009 International Association for Hydrogen Energy. Published by Elsevier Ltd. All rights reserved.
doi:10.1016/j.ijhydene.2009.01.083

Nomenclature

C	Reaction rate constant, s^{-1}
C_p	Specific heat, J/kg K
E	Activation energy, J/mol H_2
K	Permeability, m^2
m_f	Mass flow rate of the heat transfer fluid, kg/s
m	Mass flow rate of hydrogen, kg/m^3 s
M_g	Molecular weight of hydrogen, kg/kmol
n	Number of moles of hydrogen, mol
P	Pressure, bar
Q	Heat interaction, W
r_o	Outer radius of the reactor, m
R_u	Universal gas constant, J/mol K
t	Time, s
T	Temperature, K
u	Velocity, m/s
U	Overall heat transfer coefficient, W/m^2 K
V	Volume, m^3
X	Hydrogen concentration, (H/M ratio)
Z	Length of the reactor, m

Greek symbols

ϕ, ϕ_o	Slope factors
β	Hysteresis factor
ΔS	Entropy of reaction, J/mol H_2 K
ΔH	Enthalpy of reaction, J/mol H_2
ρ	Density, kg/m^3
λ	Thermal conductivity, W/m K
ε	Porosity
μ_g	Dynamic viscosity, kg/m s
ν_g	Kinematic viscosity, m^2/s

Subscripts

a	Absorption
A	High temperature reactor
B	Low temperature reactor
d	Desorption
e	Effective
eq	Equilibrium
f	Fluid, Final
fi	Heat transfer fluid inlet
fo	Heat transfer fluid outlet
g	Gas
i	Inner
m	Metal
max	Maximum
min	Minimum
P	Connecting tube
ss	Saturation solid

the system by varying the bed thicknesses, thermal conductivity and overall heat transfer coefficient. But their numerical model was limited to thin beds and did not include the effect of convection heat transfer in the energy equation. Subsequently, the same research group conducted the experiments [6] with the same metal hydride pair for comparing their numerical results. Kang and Kuznetsov [7] carried out the thermal modelling of a metal hydride chiller using $LaNi_{4.5}Al_{0.5}$/$LaNi_5$ hydride pair. Kim et al. [8] presented the thermodynamic analysis and experimental investigation of a metal hydride heat pump with different combinations of refrigeration and regeneration alloys. They showed that $Zr_{0.8}Ti_{0.2}Cr_{0.6}Fe_{1.4}$/$Zr_{0.8}Ti_{0.2}MnFe$ hydride pair provides the highest COP of about 1.59 with the refrigeration temperature near 0 °C. Fedorov et al. [9] presented the simulation of a MHHP using $LaNi_{4.5}Al_{0.25}H_x$/$TiFe_{0.8}Mn_{0.2}H_y$ hydride pair without considering the effect of hysteresis and plateau slope on the pressure concentration isotherm (PCT). Jang et al. [10] developed an unsteady one-dimensional mathematical model of MHHP system using $Zr_{0.9}Ti_{0.1}Cr_{0.9}Fe_{1.1}$/$Zr_{0.9}Ti_{0.15}Cr_{0.6}Fe_{1.45}$ hydride pair. They observed that the hydrogen pressure and hydrogen flow rate are considered to be the main controlling parameters. Recently, Ni and Liu [11] and Qin et al. [12] conducted experiments using $LaNi_{4.61}Mn_{0.26}Al_{0.13}$/$La_{0.6}Y_{0.4}Ni_{4.8}Mn_{0.2}$ hydride pair at 393–473/293–323/263–273 K (T_H/T_M/T_C) temperature range for developing air-conditioner using exhaust gas from an automobile.

Though many investigators have concentrated on the topic of metal hydride based cooling system [1–12], the commercial usage of the metal hydride heat pump does not seem to be feasible. This is probably due to poor heat and mass transfer characteristics of metal hydride and high initial cost of the alloys. The literature survey shows that most of the studies on metal hydride heat pump systems are experimental investigations [2–4,6,8,11,12]. Only few studies focused on the mathematical models [5,7,9,10]. However their scopes are limited by the use of one-dimension model without considering the effect of hysteresis and plateau slope [5,7,9,10]. Further a variation in the heat transfer fluid temperature and reactor mass are not accounted in these models.

In this paper, we present the time-dependent, two-dimensional conjugate heat and mass transfer model of the paired reactors. This model includes the effects of convective heat transfer, variation in the cooling fluid temperature along the axial direction, pressure drop inside the reactors and hysteresis effect and plateau slope in the PCT.

2. Physical model and principle of operation

Fig. 1 shows a schematic of a single-stage and single-effect MHHP used for producing the refrigeration effect at low temperature, T_C. It consists of a pair of two reactors A and B filled with $MmNi_{4.6}Al_{0.4}$ and $MmNi_{4.6}Fe_{0.4}$ hydride alloys, respectively. Dimension of each reactor is 475.0 mm length and 30.0 mm outer diameter. A filter is used at the inner most tube of 12.0 mm diameter. It distributes the hydrogen gas uniformly throughout the reactor and prevents the hydride particle from being carried away by the hydrogen gas during the desorption process. Metal hydride is filled in the space between the inner tube and the filter section. The cooling fluid flows around the outer periphery of the tube of 1.5 mm gap. These two reactors are coupled by a connecting tube with a control valve through which hydrogen gas can flow freely between the reactors when the valve is opened. The dimensions of the connecting tube are taken as 300.0 mm length and

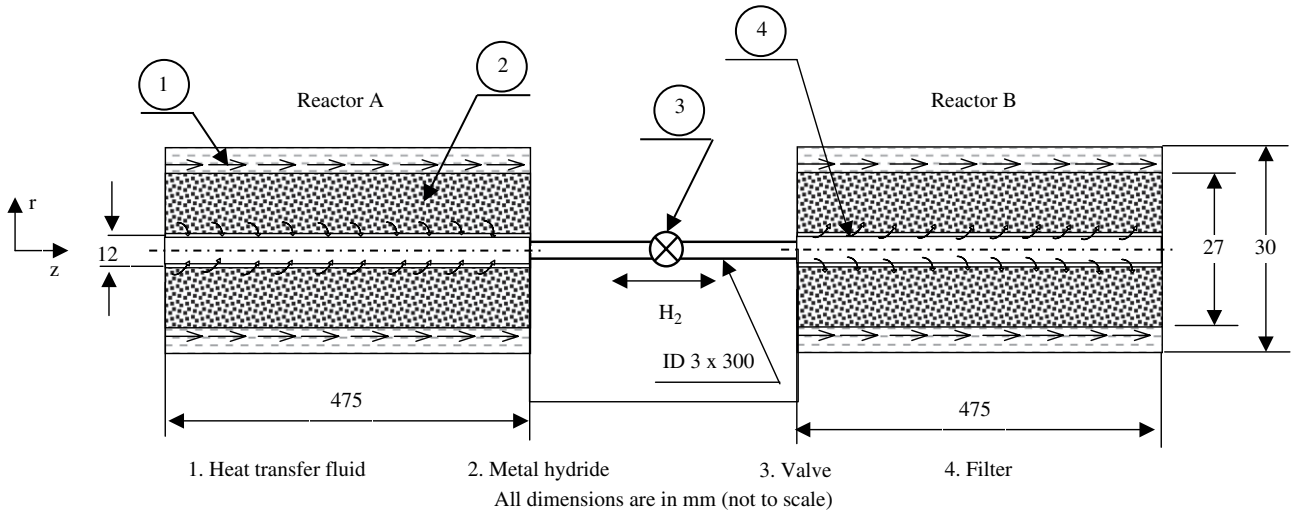


Fig. 1 – Schematic diagram of coupled metal hydride reactors.

3.0 mm internal diameter. Fig. 2 shows the operating cycle on the van't Hoff plot. It consists of four processes and they are explained below.

2.1. *Process* ab

Initially, the reactor A is fully hydrided (X_{max}) and B is fully dehydrided (X_{min}) at their respective operating temperatures of T_H and T_M. Two reactors are coupled by a connecting tube with a valve (Fig. 1). Since the operating valve is initially closed, the equilibrium pressure difference exists between the reactors. Once the valve is opened, due to the difference in pressure, hydrogen gas starts to desorb from the reactor A by taking heat from the reaction bed and heat transfer fluid, and reactor B starts to absorb hydrogen gas by rejecting the heat of absorption to the reaction bed and heat transfer fluid. This process continues till the fixed amount of hydrogen gas transfers from reactor A to reactor B.

2.2. *Process* bc

During this process, the valve between reactors A and B is closed and no hydrogen transfer between the reactors takes place. Only the heat transfer takes place between the hydride bed and the cooling/heating fluids. This process is continued till the reactors A and B reach T_M and T_C, respectively.

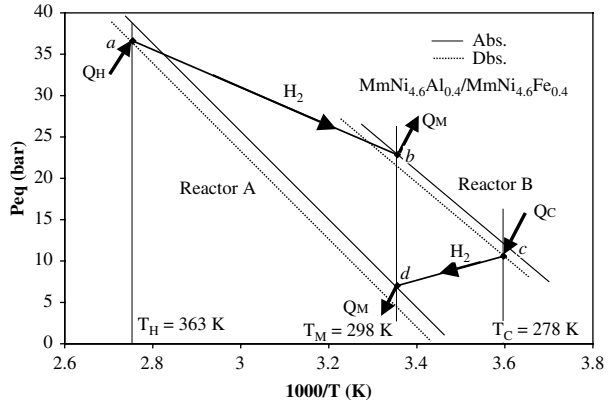


Fig. 2 – van't Hoff plot for a single-stage and single-effect metal hydride heat pump.

2.3. *Process* cd

Once the reactors A and B reach the medium and low (refrigeration) temperatures, the valve between the reactors is opened. Due to the existence of pressure difference, the hydrogen starts to desorb from the reactor B at temperature T_C by extracting the heat of desorption from the reaction bed and heat transfer fluid, yielding refrigeration effect. Simultaneously, the hydride A absorbs this hydrogen by rejecting the heat of absorption to the reaction bed and cooling fluid at the medium temperature, T_M. This process continues till the fixed amount of hydrogen is transferred (same as during process *ab*).

2.4. *Process* da

During this process the valve is closed. Reactors A and B are sensibly heated to T_H and T_M, respectively. Thus a first cycle operation is completed.

3. Problem formulation

The dependence of the equilibrium pressure, $P_{eq,}$ on the reciprocal of the absolute temperature, 1/T, which is an important characteristic of the two hydrides, is shown in Fig. 2. A pair of hydrides to be used in a heat pump should be selected according to the required range of equilibrium pressure conditions at points a, b, c and d at the design high, medium and low temperatures T_H, T_M and T_C, respectively (Fig. 2). Table 1 shows the enthalpy and entropy of reactions of the selected metal hydride pair during both absorption and desorption processes.

The following assumptions are made in the modeling.

Table 1 – Thermo-physical properties of metal hydride alloys.

Alloys	ΔH (kJ/mol H_2)		ΔS (J/mol H_2 K)	
	Absorption	Desorption	Absorption	Desorption
$MmNi_{4.6}Al_{0.4}$	−29.0	−27.8	−108.7	−107.2
$MmNi_{4.6}Fe_{0.4}$	−25.2	−24.7	−104.5	−105.4

1. Hydrogen is considered to be a perfect gas.
2. Initially at process *ab*, the hydride beds of reactors A and B are in equilibrium with hydrogen gas.
3. Heat transfer through the hydride bed is assumed by two-dimensional conduction and convection. The effect of radiation is negligible.
4. The thermo-physical properties of the metal hydride, such as, reaction enthalpy and entropy, thermal conductivity and specific heat capacity are independent of temperature, concentration and hydrogen pressure.
5. Pressure and temperature inside the connecting tube are independent of space but are time dependent.
6. The reactors are assumed to be well insulated and no heat transfer takes place between them and to the surroundings.

Initially, the system is in equilibrium which depends upon the temperature and concentration of the hydrides. The equilibrium pressures of the reactors are calculated using van't Hoff equation [1].

$$P_{eq} = 10^5 \exp\left[\frac{\Delta H}{R_u T} - \frac{\Delta S}{R_u} + (\phi \pm \phi_o)\tan\left[\pi\left(\frac{X}{X_f} - \frac{1}{2}\right)\right] \pm \frac{\beta}{2}\right] \quad (1)$$

where, ϕ and ϕ_o denote the slope factors and β the hysteresis factor, '+' and '−' denote the absorption and desorption processes, and X and X_f denote the concentration at the given time (t) and final concentrations of the hydrogen.

Gas pressure and temperature in the connecting tube immediately after opening the valve are given by

$$P_{g,P} = \frac{P_{g,A}V_A + P_{g,B}V_B}{V_A + V_B} \quad (2)$$

$$T_{g,P} = \frac{n_A T_A + n_B T_B}{n_A + n_B} \quad (3)$$

where, $P_{g,A}$, V_A, $P_{g,B}$ and V_B are the gas pressures and volumes of the reactors A and B, respectively. Since the hydrogen is assumed to be a perfect gas, the number of moles of hydrogen in reactors A and B are calculated using the perfect gas law

$$n_A = \frac{P_A V_A}{R_u T_A}; \quad n_B = \frac{P_B V_B.}{R_u T_B} \quad (4)$$

The number of moles of hydrogen and gas temperature and pressure in the connecting tube at any time during the hydrogen transfer (absorption and desorption processes) are calculated using the following equations

$$n_{g,t+\delta t} = n_{g,t} + n_d - n_a \quad (5)$$

$$T_{g,t+\delta t} = \frac{(n_{g,t} - n_a)T_{g,a} + n_d T_{g,d}}{n_{g,t} - n_a + n_d} \quad (6)$$

$$P_{g,t+\delta t} = \frac{n_{g,t+\delta t} R_u T_{g,t+\delta t}}{V_A + V_B + V_P} \quad (7)$$

$n_{g,t}$, n_d and n_a respectively denote the number of moles of hydrogen in the connecting tube immediately after opening the valve, number of moles of hydrogen desorbed from the reactor A and number of moles of hydrogen absorbed in reactor B during time $t = \delta t$.

As stated in the physical model, the operating cycle consists of two hydrogen transfer processes (*ab* and *cd*) and two sensible heat transfer processes (*bc* and *da*). The heat and mass transfer rates during the processes *ab* and *cd* are estimated by simultaneously solving continuity, momentum and energy equations in both the reactors. The heat transfer rates during the processes *bc* and *da* are estimated by solving only the energy equation.

3.1. Process ab

During this process, hydrogen is desorbed from the reactor A by taking the heat of desorption from the heat transfer fluid at T_H and absorbed at reactor B by releasing the heat of absorption to the heat transfer fluid at T_M. The computational modelling of this process is discussed below.

3.1.1. Reactor A (desorption)

Mass flux (mass flow rate per unit volume) during the desorption of hydrogen is given by [16]

$$m_A = C_d \exp\left(\frac{-E_d}{R_u T_A}\right)\left(\frac{P_{eq,A} - P_{g,t+\delta t}}{P_{eq,A}}\right)\rho_{m,A} \quad (8)$$

where, $\rho_{m,A}$ is the density of hydride at any given time t and P_g is the gas pressure in the connecting tube at any given time found in Eq. (7).

Assuming thermal equilibrium between the hydride bed and hydrogen, a combined energy equation is considered instead of separate equations for both solid and gaseous phases [13]:

$$(\rho C_p)_e \frac{\partial T}{\partial t} + (\rho C_p)_g \vec{u}.\nabla T = \lambda_e \nabla^2 T - m_A\left[\frac{\Delta H}{M_g} - T(C_{p,g} - C_{p,m})\right] \quad (9)$$

where

$$(\rho C_p)_e = (\varepsilon \rho C_p)_g + ((1-\varepsilon)\rho C_p)_m \quad (10)$$

and the effective thermal conductivity

$$\lambda_e = \varepsilon\lambda_g + (1-\varepsilon)\lambda_m. \quad (11)$$

The hydrogen mass balance is expressed as

$$\varepsilon\frac{\partial(\rho_g)}{\partial t} + \nabla(\rho_g \overrightarrow{u_g}) = m_A \quad (12)$$

where ρ_g denotes the density of the hydrogen gas in the reactor A during the desorption process. Hydrogen density is determined using the perfect gas law. Velocity of hydrogen gas (u_g) is calculated using the Darcy's law [13]

$$\overrightarrow{u_g} = -\frac{K}{\mu_g}\nabla P_g \quad (13)$$

By substituting the density (ρ_g) and velocity (u_g) of the gas in Eq. (12) the gas pressure (P_g) inside the reactors are determined using the following equation

$$\left(\frac{\varepsilon M_g}{R_u T}\right)\frac{\partial P_g}{\partial t}+\left(\frac{\varepsilon M_g P_g}{R_u}\right)\frac{\partial}{\partial t}\left(\frac{1}{T}\right)-\frac{K}{\nu_g r}\frac{\partial}{\partial r}\left(r\frac{\partial P_g}{\partial r}\right)-\frac{K}{\nu_g}\frac{\partial}{\partial z}\left(\frac{\partial P_g}{\partial z}\right)=m_A. \tag{14}$$

3.1.1.1. *Initial and boundary conditions*. Initially at time $t=0$, the density of the metal hydride, temperatures of the metal hydride and hydrogen gas and hydride concentration are assumed to be uniform throughout the reactor

$$\rho_{m,A}(z,r)=\rho_{ss};\ \ T_{m,A}(z,r)=T_{g,A}(z,r)=T_H;\ \ X_A(z,r)=X_{max,A}. \tag{15}$$

The left and right boundaries of the reactors are assumed to be adiabatic

$$\frac{\partial T}{\partial z}(z,r,t)_{z=0}=0;\quad \frac{\partial T}{\partial z}(z,r,t)_{z=Z}=0 \tag{16}$$

and at bottom wall (along the porous filter)

$$P_g(z,r_i,t)=P_g. \tag{17}$$

The cooling fluid flows through the outer peripheral tube and therefore the convective boundary condition is applied at $r=r_o$

$$-\lambda_e\frac{\partial T}{\partial r}(z,r_o,t)=U\left(T_{z,r_o,t}-T_f\right) \tag{18}$$

where, $T_{(z,r_o,t)}$ and T_f are the temperatures of the hydride bed at the outer radius and heat transfer fluid, respectively.

In the above-mentioned boundary condition, the variation of cooling fluid temperature along the axial direction is negligible. However, in the practical case the cooling fluid temperature varies along the axial direction. Therefore in the present work, the variable wall temperature condition is also considered using the following equation [17]

$$\frac{dQ}{dt}=m_f C_{p,f}\left(T_{fo}-T_{fi}\right). \tag{19}$$

The heat transfer rate is proportional to the mass flow rate and difference in the cooling fluid inlet and outlet temperatures. The heat transfer rate can also be calculated by using the logarithmic mean temperature difference method [18]. By equating these two equations, the temperature variation of the cooling fluid in the axial direction can be calcuated using the following equation

$$T_{fo}=T_{fi}+\left[T_{z,r_o,t}-T_{fi}\right]\left[1-\exp\left(-\frac{UA}{m_f C_{p,f}}\right)\right]. \tag{20}$$

3.1.2. *Reactor B (absorption)*

The mass flux of hydrogen absorbed is expressed as [16]

$$m_B=C_a\exp\left(\frac{-E_a}{R_u T_B}\right)\ln\left(\frac{P_{g,t+\delta t}}{P_{eq,B}}\right)(\rho_{ss}-\rho_{m,B}). \tag{21}$$

The equilibrium pressure is calculated from Eq. (1). The rise in temperature of the reactor B is found out by using the energy equation as given below

$$(\rho C_p)_e\frac{\partial T}{\partial t}+(\rho C_p)_g\vec{u}.\nabla T=\lambda_e\nabla^2 T+m_B\left[\frac{\Delta H}{M_g}-T(C_{p,g}-C_{p,m})\right]. \tag{22}$$

The hydrogen mass balance during the absorption in the reactor B is expressed as

$$\varepsilon\frac{\partial(\rho_g)}{\partial t}+\nabla\left(\rho_g\overrightarrow{u_g}\right)=-m_B. \tag{23}$$

Hydrogen gas pressure in the reactor B is found in the same way as for reactor A using Eq. (14).

3.1.2.1. *Initial and boundary conditions*. Initial conditions of the reactor B at time $t=0$ are given as

$$\rho_{m,B}(z,r)=\rho_i;\quad T_{m,B}(z,r)=T_{g,B}(z,r)=T_M;\quad X_B(z,r)=X_{min,B}. \tag{24}$$

The boundary conditions used in the reactor A are the same as for the reactor B. The initial condition stated above is used only at the first cycle.

3.2. *Process* bc

During this process, only the sensible heat transfer takes place between the hydride bed and the heat transfer fluid and no mass transfer takes place. Therefore, the governing equations for reactors A and B become

$$(\rho C_p)_e\frac{\partial T}{\partial t}+(\rho C_p)_g\vec{u}.\nabla T=\lambda_e\nabla^2 T. \tag{25}$$

The initial conditions of the sensible cooling processes are used as the final conditions of the previous desorption/absorption process.

3.3. *Process* cd

During this process, hydrogen is transferred from reactor B to reactor A at low pressure. The initial condition of this process is the final condition of the process *bc* of the respective reactors. The governing equations and boundary conditions used in this process are similar to those for process *ab*.

3.4. *Process* da

In the sensible heating process, the reactors A and B are heated to temperatures T_H and T_M, respectively. The final condition of this process is the initial condition of the next cycle of process *ab*.

4. Solution methodology

The solution of the above-mentioned mathematical model is obtained using the fully implicit finite volume method. The solution procedure of this system begins with the process *ab* and ends with the process *da*, so that the simulation of one complete cycle is carried out. Initially, the metal hydride heat pump is in the equilibrium and pressures inside the reactors A and B are found using Eq. (1). Once the valve is opened, hydrogen gas is desorbed from the reactor A and it is absorbed in the reactor B. This process is continued until a predefined quantity of hydrogen gas is desorbed from reactor A. The coupled heat and mass transfer processes (*ab* and *cd*) are assumed to be converged when the difference between the

predefined amount of hydrogen and cumulative amount of hydrogen transfer is less than 0.0001 g. The sensible heat transfer processes (*bc* and *da*) are assumed to be converged when the difference between the heat transfer fluid temperature and average bed temperature is less than 0.1 K. To find the variation in cycle time for both constant and variable wall temperature boundary conditions the average hydride bed temperature is calculated at $z/Z = 0.95$. The end conditions of the sensible heating process are taken as the initial conditions of the first process of the next cycle. The cycle is repeated (minimum 10 cycles) till processes reach stable state and then the computed values are presented.

Fig. 3 shows the grid independence study by considering the effect of three different grid sizes on the concentrations in reactors A and B. It can be concluded that there is no significant change in the profile for a grid size more than 41×41. Hence the results reported in the subsequent section are by using the grid size of 41×41.

Table 2 – Design and operating data, properties and constants used for numerical analysis.

High/low temperature hydride bed	$MmNi_{4.6}Al_{0.4}/MmNi_{4.6}Fe_{0.4}$
High temperature (T_H)	363 K
Medium temperature (T_M)	298 K
Low temperature (T_C)	278 K
Effective thermal conductivity (λ_e)	1.6 W/m K
Porosity (ε)	0.5
Specific heat capacity (C_p)	419 J/kg K
Density of solid (ρ_m)	8400 kg/m^3
Bed thickness ($r_o - r_i$)	0.0075 m
Mass flow rate of heat transfer fluid (m_f)	0.006944 kg/s
Properties of hydrogen	
Thermal conductivity of hydrogen (λ_g)	0.127 W/m K
Specific heat of hydrogen ($C_{p,g}$)	14,283 J/kg K
Density of hydrogen (ρ_g)	0.0838 kg/m^3

5. Results and discussion

The $MmNi_{4.6}Al_{0.4}/MmNi_{4.6}Fe_{0.4}$ hydride pair is chosen for the detailed investigation of a single-stage and single-effect MHHP because the reaction kinetics data of the two hydrides are relatively well known and these hydrides are appropriate in the required temperature ranges. Hydrogen absorption/desorption characteristics for these two alloys have already been studied [14,15,17]. Design and operating data, properties and constants used for the present computational study of the two hydrides are reported in Table 2.

5.1. *Validation of mathematical model*

For the validation purpose, the reactor geometry used by Ni and Liu [11] is chosen and mathematical modelling is performed accordingly. The hysteresis and plateau slope of the PCT for the corresponding high and low temperature alloys are determined from the experimental data reported by Ni and Liu [11]. The cycle time for the processes at different heat source temperatures, thermal conductivity and bed thickness of the reactors are selected based on the experimental conditions reported by Ni and Liu [11]. Figs. 4 and 5 show that the predicted temperature profiles of the regeneration and refrigeration alloys at different source temperatures ranging from 388 K to 423 K for $LaNi_{4.61}Mn_{0.26}Al_{0.13}/La_{0.6}Y_{0.4}Ni_{4.8}Mn_{0.2}$ hydride pairs match reasonably well with the experimental data of Ni and Liu [11]. A small deviation between the present computations and the experimental data is due to the assumed values of the reaction rate constant and the experimental uncertainties used in the present study. These data are not reported in the literature [11].

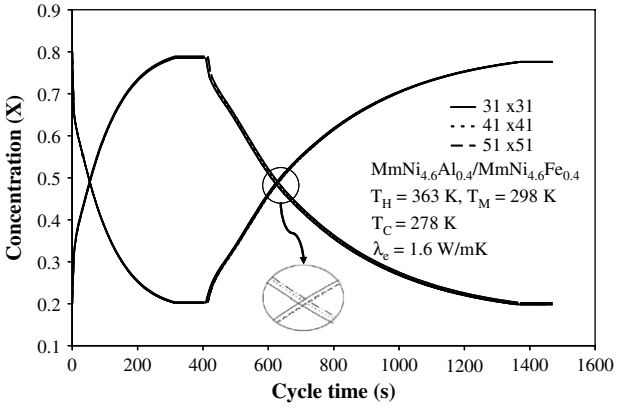


Fig. 3 – Grid independent test.

5.2. *Effect of convective boundary conditions on the hydrogen absorption and desorption rates*

Fig. 6 shows the variations of hydride concentrations in reactors A and B over a cycle for both constant and variable wall temperature boundary conditions. The concentration limits are fixed based on the PCT plot so that the minimum desorption hydride pressure of hydride A at T_H is higher than the maximum absorption pressure of hydride B at T_M. Based on the above-mentioned conditions the concentration limits are fixed as 0.2–0.8. It is observed from Fig. 6 that the model

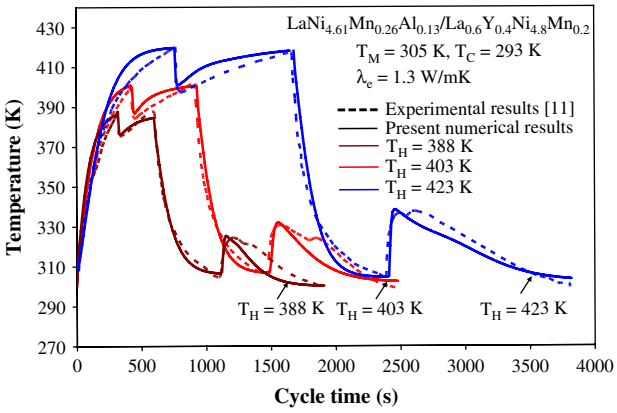


Fig. 4 – Validation of the predicted regeneration alloy reaction bed temperature profiles at different source temperatures.

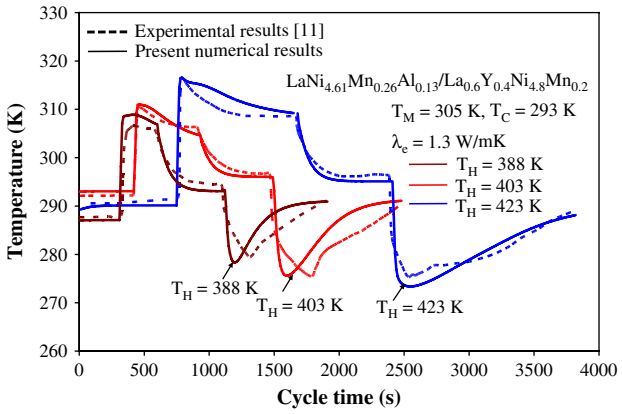


Fig. 5 – Validation of the predicted refrigeration alloy reaction bed temperature profiles at different source temperatures.

with the variable wall temperature condition takes 1765.6 s for completing a cycle, whereas the model with the constant wall temperature condition takes only 1470 s.

It is seen that for the constant wall temperature boundary condition, the average concentration inside the reactor varies only in the radial direction. However in the variable wall temperature boundary condition, pressure, concentration and bed temperature vary in both axial and radial directions [17]. During process *ab*, the hydrogen starts to desorb in the reactor A in its high temperature regions and hence, hydrogen starts flowing towards the filter. Due to the supply of heat transfer fluid from the left boundary, the reactor temperature is higher on the left boundary than that on the right boundary. Hence, the concentration decreases faster on the left boundary than on the right boundary. Therefore, the desorption for the variable wall temperature condition takes more time than that in the constant wall temperature boundary condition. It is observed from Fig. 6 that desorption of hydrogen (during process *ab*) at high temperature is faster than that at low temperature (during process *cd*). This is because the pressure difference in process *ab* is much higher than that during the process *cd*. Therefore, the reaction rate is faster and change in concentration with time is sharper during the first half cycle. For a given effective thermal conductivity, bed thickness and specific heat capacity, the time taken for sensible heat transfer processes are calculated. Times taken for all the processes are listed in Table 3. The difference in cycle times for the constant and variable wall temperature boundary conditions is found to be approximately 5 min.

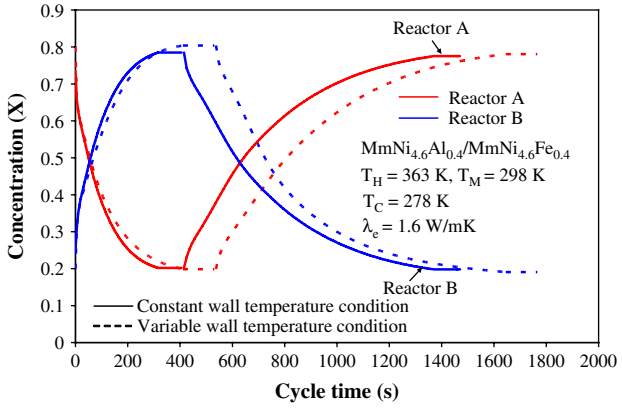


Fig. 6 – Effect of convective boundary conditions on hydride concentrations.

5.3. *Effect of convective boundary conditions on the hydride bed temperature*

Fig. 7 shows the variation in average bed temperatures of high and low temperature reactors over a cycle. It is observed that due to the poor thermal conductivity of the hydride bed the required amount of heat is not transferred from/to the heat transfer fluid. Hence the fall/rise in temperature of the reactor bed occurs as soon as the process starts, and it reaches the heat transfer fluid temperature gradually. It is observed that the difference in the equilibrium pressure between the reactors leads to rise/drop in temperature at the initial stages. The lowest average bed temperature obtained in process *cd* at reactor B for the constant and variable wall temperature boundary conditions are 271 K and 269.1 K, respectively.

5.4. *Effect of convective boundary conditions on the hydride equilibrium pressures*

Fig. 8 shows the hydrogen pressures in reactors A and B for both constant and variable wall temperature boundary conditions. Initially the system is in equilibrium with respect to the reactors A and B. Once the valve between the reactors is opened, due to the pressure difference, hydrogen starts to desorb from the reactor A and it is absorbed in the reactor B by releasing heat of absorption. This process continues till both the pressures reach the equilibrium condition as illustrated in Fig. 8. It is observed from Fig. 8 that this process terminates at 15 bar at the end of 315 s for the constant wall temperature condition and 411 s for the variable wall temperature boundary condition.

During the sensible cooling process, the reactor A cools down from 363 K to 298 K and similarly reactor B cools from 298 K to 278 K. Hence the pressures of the high and low temperature reactors decrease to 2.1 and 7.2 bar, respectively.

Table 3 – Comparisons of cycle time for constant and variable wall temperature boundary conditions.

Sl. No	Processes	Constant wall boundary condition (s)	Variable wall boundary condition (s)	Difference in time (s)
1	Process *ab*	315.1	411	95.9
2	Sensible cooling (Process *bc*)	99.9	126.3	26.4
3	Process *cd*	954.8	1108.3	153.5
4	Sensible heating (Process *da*)	100.2	120	19.8
	Total cycle time	**1470 s**	**1765.6 s**	**295.6 s**

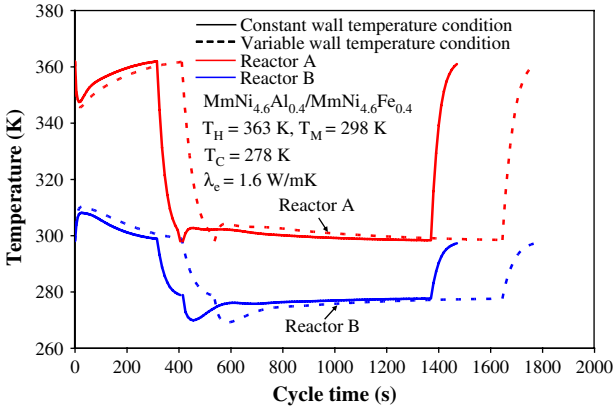


Fig. 7 – Effect of convective boundary conditions on hydride bed temperatures.

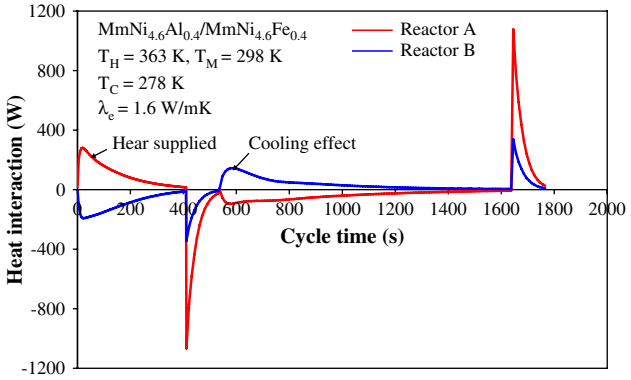


Fig. 9 – Effect of convective boundary conditions on heat interactions.

Similarly, in process *cd* the hydrogen transfer takes place from B to A. This process terminates when both the reactors reach the equilibrium condition. Finally the heating process completes the cycle and the pressures of reactors reach the initial condition for continuing the next cycle.

5.5. *Effect of convection boundary conditions on heat interaction*

The heat interaction (cooling/heating) between hydride bed and heat transfer fluid for a complete cycle time is shown in Fig. 9. Initially, the variation in the heat transfer fluid temperature is zero. Due to the exothermic/endothermic processes, heat is carried away/supplied to the reactors and their temperatures increase/decrease drastically and become zero at the end of the processes. It is observed from Fig. 9 that the change in the heat transfer fluid temperature during the process *ab* reaches the maximum value within 20 s. The maximum fall and rise in the fluid temperatures between inlet and outlet of the reactors A and B are 9.6 K and 6.5 K (corresponding to the heat interactions of 278 W and 188 W), respectively. Similarly in process *cd*, the maximum rise and fall in fluid temperatures at reactor A and B are 3.3 K and 5 K, respectively, at 587 s. In the processes *ab* and *cd*, the heat of desorption is more than the heat of absorption. This is mainly due to the heat interaction that takes place at around atmospheric conditions during the absorption of hydrogen at processes *ab* and *cd*.

5.6. *Dynamic PCT characteristics of the metal hydride heat pump*

The actual dynamic behaviour of metal hydride heat pump considering the variable wall temperature boundary condition under the operating temperature limits of 363/298/278 K is illustrated in Fig. 10. A large deviation between the dynamic and static van't Hoff plots is observed. It is seen from Fig. 10 that the path followed in the high temperature and low temperature reactors are indicated as ABCDEFA and abcdefa, respectively. ABC shows the dehydriding process, CD the sensible cooling, DEF the hydriding and FA the sensible heating process. Similarly the hydriding, cooling, dehydriding and heating processes are represented in reactor B. Initially during the dehydriding process ABC, the pressure, temperature and concentration decrease drastically. The temperature of the hydride bed increases and reaches the heat transfer fluid temperature gradually as shown in Fig. 10. But the pressure still decreases and reaches the pressure equilibrium

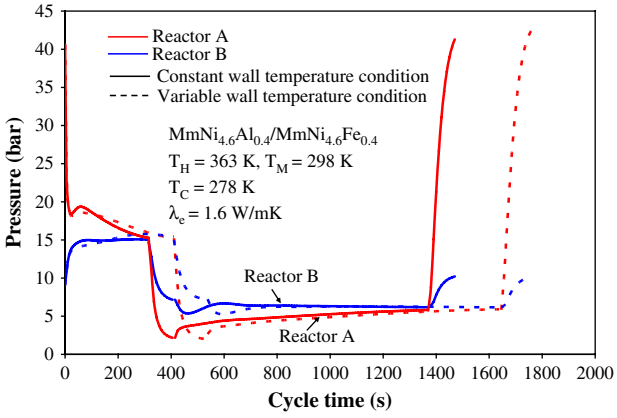


Fig. 8 – Effect of convective boundary conditions on hydride bed pressures.

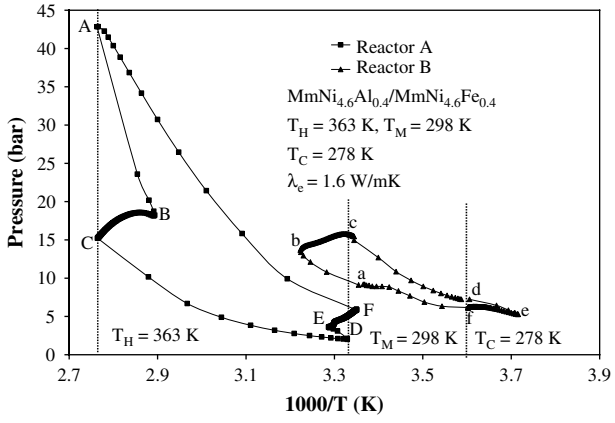


Fig. 10 – Dynamic van't Hoff plot of the heat pump.

with low temperature reactor. Fig. 10 shows that the pressures at points C and c are approximately equal to 15 bar. At the same time the concentration in the high temperature reactor decreases to 0.2. Similarly, the changes in pressure, temperature and concentration at low temperature reactor are shown in Fig. 10 at points a–b–c. During the sensible heat transfer processes (cooling/heating) the concentration remains same for both the reactors. At the end of the sensible cooling process, pressures at reactors A and B are indicated at point D and d, respectively. When the valve between the two hydride beds is opened, dehydriding starts at low temperature reactor indicated by d–e–f. The lowest temperature obtained at point e is 269.1 K. This process stops when both the reactor pressures reach the equilibrium condition as shown in Fig. 10 at points F and f. During the process *da*, hot fluids are supplied to the reactors A and B for rising their temperatures to T_H and T_M, respectively.

6. Conclusions

A computational study of a metal hydride heat pump working with $MmNi_{4.6}Al_{0.4}/MmNi_{4.6}Fe_{0.4}$ hydride pair is presented. A comparison is performed between the computations and experimental data reported in the literature for the high temperature and low temperature reactors for a complete cycle at different heat source temperatures ranging from 388 K to 423 K. A reasonably good agreement between the two was observed. The effects of the constant and variable wall temperature boundary conditions on the hydrogen concentration and pressures at two reactors are studied. The computations reveal that the difference in cycle times for the constant and variable wall temperature boundary conditions is found to be approximately 5 min for 363/298/278 K operating temperatures. The lowest refrigeration temperature obtained is 269.1 K for the variable wall temperature boundary condition. The actual dynamic van't Hoff plot of the metal hydride heat pump is studied. A large deviation is observed between the static and dynamic van't Hoff plots. The heat interaction (cooling/heating) between the hydride bed and heat transfer fluids is also studied for a complete cycle.

Acknowledgements

The authors thank Prof. M. Groll, University of Stuttgart, Germany for his valuable suggestions.

REFERENCES

[1] Nishizaki T, Miyamoto K, Yoshida K. Coefficients of performance of hydride heat pumps. J Less-Common Metals 1983;89:559–66.
[2] Ron M. A hydrogen heat pump as a bus air conditioner. J Less-Common Metals 1984;104:259–78.
[3] Bjurstrom H, Suda S. The metal hydride heat pump: dynamics of hydrogen transfer. Int J Hydrogen Energy 1989; 14(1):19–28.
[4] Lee SG, Kim YK, Lee JY. Operating characteristics of metal hydride heat pump using Zr-based laves phases. Int J Hydrogen Energy 1995;20(1):77–85.
[5] Gopal MR, Murthy SS. Prediction of metal–hydride refrigerator performance based on reactor heat and mass transfer. Int J Hydrogen Energy 1995;20(7):607–14.
[6] Gopal MR, Murthy SS. Experiments on a metal hydride cooling system working with ZrMnFe/$MmNi_{4.5}Al_{0.5}$ pair. Int J Refrig 1999;22:137–49.
[7] Kang BH, Kuznetsov A. Thermal modelling and analysis of a metal hydride chiller for air conditioning. Int J Hydrogen Energy 1995;20(8):665–74.
[8] Kim KJ, Feldman KT, Razani A. Heat-driven hydride slurry heat pumps. Int J Refrig 1997;20(5):339–51.
[9] Fedorov EM, Shanin YI, Izhvanov LA. Simulation of hydride heat pump operation. Int J Hydrogen Energy 1999;24:1027–32.
[10] Jang KJ, Fateev GA, Park JG, Han SC, Lee P, Lee JY. Simulation of the metal hydride heat pump system with the single and double reactors. Int J Hydrogen Energy 2001;26:231–41.
[11] Ni J, Liu H. Experimental research on refrigeration characteristics of a metal hydride heat pump in auto air-conditioning. Int J Hydrogen Energy 2007;32:2567–72.
[12] Qin F, Chen J, Lu M, Chen Z, Zhou Y, Yang K. Development of a metal hydride refrigeration system as an exhaust gas-driven automobile air conditioner. Renew Energ 2007;32:2034–52.
[13] Jemni A, Nasrallah BS. Study of two-dimensional heat and mass transfer during absorption in a metal–hydrogen reactor. Int J Hydrogen Energy 1995;20(1):43–52.
[14] Muthukumar P, Maiya MP, Murthy SS. Experiments on a metal hydride-based hydrogen storage device. Int J Hydrogen Energy 2005;30:1569–81.
[15] Muthukumar P, Madhavakrishna U, Dewan A. Parametric studies on a metal hydride based hydrogen storage device. Int J Hydrogen Energy 2007;32:4988–97.
[16] Mayer U, Groll M, Supper W. Heat and mass transfer in metal hydride reaction beds: experimental and theoretical results. J Less-Common Metals 1987;131:235–44.
[17] Muthukumar P, Ramana SV. Numerical simulation of coupled heat and mass transfer in metal hydride-based hydrogen storage reactor. J Alloy Comp, in press.
[18] Incropera FP, DeWitt DP. Fundamentals of heat and mass transfer. 4th ed. New York: John Wiley & Sons; 1998. p. 581–632.